INSTITUTE OF PHYSICS PUBLISHING SMART MATERIALS AND STRUCTURES
Smart Mater. Struct. **12** (2003) 524–532 PII: S0964-1726(03)63039-9

Numerical modeling of a damaged plate with piezoelectric actuation

Y Y Li, L Cheng, L H Yam and Y J Yan

Department of Mechanical Engineering, The Hong Kong Polytechnic University, Hung Hom, Kowloon, Hong Kong SAR, China

Received 3 July 2002, in final form 15 January 2003
Published 25 June 2003
Online at stacks.iop.org/SMS/12/524

Abstract
In this paper, the numerical modeling of a damaged plate with piezoelectric actuation is presented. Unlike in previous studies, the effects of the defect are considered and embodied by mass and stiffness reductions in the equation of motion. The model is validated using indices related to frequency variation and energy change in both frequency and time domains. A comparison of the tendencies of the measured indices with those of the simulated ones shows a reasonably good agreement. Results show that the energy index is more sensitive to damage than the frequency index. Both square-wave and pseudo-random excitations can be used to assess the energy index variation. For the latter, however, an averaging over time signals is needed to provide more reliable results.

(Some figures in this article are in colour only in the electronic version)

1. Introduction

A plate with an active device is one kind of intelligent structure used extensively in the field of vibration analysis, vibration control, and damage detection. In such structures, piezoelectric materials are frequently used as actuators/sensors due to their intrinsic direct and converse piezoelectric effects (Bhattacharya *et al* 1998, Heyliger and Saravanos 1995, Lam and Ng 1999, Wang *et al* 2001, Jian *et al* 1997). Structural modeling, as the foundation for analyzing these issues, has attracted much attention and led to the development of various approaches based on the classical laminate theory (Chandrashekhara *et al* 1998, Agrawal *et al* 1994), first-order shear deformation theory (Qu 2001, Banks *et al* 1995), layer-wise theory (Barbero and Reddy 1991), higher-order theory (Chee *et al* 1999), etc. Recent surveys reported by Gopinathan *et al* (2000), Benjeddou (2000) and Chee *et al* (1998) show that an extensive effort on the modeling of plate-like structures has been made to establish efficient numerical and experimental tools.

In the structural modeling, a matter of significant concern is the modeling of a damaged plate with piezoelectric actuation. Since any damage occurring in a structure modifies its dynamic characteristics, an accurate identification of the damage (size, location, and depth) usually requires a large number of tests, and hence has a high cost. For this reason, it is desirable to develop numerical models, which are accurate enough to predict changes due to damage. Comparing with the modeling of plates without damage, however, the work reported on the modeling of damaged plates with piezoelectric actuation is still quite limited due to the complication at the interface between the damage and the structure. Ostachowicz and Krawczuk (2001) gave a review on the modeling methods for composite structures with delamination or cracks, in which continuous, discrete–continuous, and discrete models have been described. Banks *et al* (1997) modeled a clamped plate-like structure with non-symmetrical damage, in which the weak and strong formulations of the equations of motion were presented in detail. Chattopadhyay *et al* (1999) analyzed the dynamics of delaminated composite plates with piezoelectric actuators, and a refined higher-order-theory-based finite-element model was developed. These results are useful for the modeling of a damaged plate. However, the dynamic effect of damage and piezoelectric patches on the modeling is seldom discussed quantitatively.

In this paper, the numerical modeling of a damaged plate with piezo-ceramic patches is presented. Using the variational approach, the equation of motion is derived, and the effect of damage is embodied by the reductions of mass and stiffness matrices. In order to validate the model, an index related to energy variation is proposed, in addition to the conventional frequency index. Whilst the latter is very intuitive for quantifying the frequency change due to the damage, the former requires a wavelet decomposition to quantify the energy

change in each frequency band. These two indices are used in both numerical simulations and experiments. Comparison shows that the proposed model is accurate enough to predict the general tendency of these two indices when damage occurs in the plate. It can potentially provide an alternative tool for constructing a database for damage detection of plate-like structures using the simulated model instead of doing a large amount of laboratory work.

2. Modeling of a damaged plate

This section is an extension of the previous work by Proulx and Cheng (2000), in which the variational approach is used to construct a structural model by means of the Lagrange equations. During the modeling analysis, the coupling between the plate and PZT is considered, and the electromechanical effects of piezo-elements such as mass, stiffness, and actuation are included in the model. In order to simplify the formulation procedure, the following assumptions are made:

(A1) Damage in the plate is simulated by a defective area with a small thickness reduction to ensure linear strain distribution through the thickness and zero transverse shear stresses.

(A2) Perfect bonding is assumed, between the plate and the piezoelectric elements, with zero glue thickness. This leads to a continuity of the displacement and the transverse stresses at the interface.

Consider a rectangular plate ($2a \times 2b \times 2h$) with bonded piezoelectric patches in the region $\Omega_{pe} : \{x_{pe1} \leqslant x \leqslant x_{pe2}, y_{pe1} \leqslant y \leqslant y_{pe2}\}$ on both sides of the structure, with a damage occurring at $\Omega_d : \{x_{d1} \leqslant x \leqslant x_{d2}, y_{d1} \leqslant y \leqslant y_{d2}\}$ as shown in figure 1. The two piezoelectric patches are driven in anti-phase to create effects of bending of the plate. In light of the Kirchhoff's assumption and the assumption (A2) mentioned above, the strain can be written as

$$\{\varepsilon\}_{pl} = \begin{Bmatrix} \varepsilon_x^{pl} \\ \varepsilon_y^{pl} \\ \varepsilon_{xy}^{pl} \end{Bmatrix} = \begin{Bmatrix} -z\frac{\partial^2 w(x,y,t)}{\partial x^2} \\ -z\frac{\partial^2 w(x,y,t)}{\partial y^2} \\ -2z\frac{\partial^2 w(x,y,t)}{\partial x\,\partial y} \end{Bmatrix} \tag{1}$$

for the plate, and

$$\{\varepsilon\}_{pe} = \frac{V_{pe}}{h_{pe}} \begin{Bmatrix} d_{31} \\ d_{32} \\ 0 \end{Bmatrix} \tag{2}$$

for the piezoelectric actuator, where $w(x, y, t)$ denotes the mid-plane transverse displacement of point (x, y) on the plate, h_{pe} is the thickness of the piezoelectric patch, and V_{pe} is the applied voltage on the top and bottom patches. d_{31} and d_{32} are the piezoelectric strain coefficients. Correspondingly, the stresses for the plate and the piezoelectric actuator are expressed by Fuller *et al* (1996)

$$\{\sigma\}_{pl} = \frac{E_{pl}}{1-\nu_{pl}^2} \begin{bmatrix} 1 & \nu_{pl} & 0 \\ \nu_{pl} & 1 & 0 \\ 0 & 0 & \frac{(1-\nu_{pl})}{2} \end{bmatrix} \begin{Bmatrix} \varepsilon_x^{pl} \\ \varepsilon_y^{pl} \\ \varepsilon_{xy}^{pl} \end{Bmatrix} \tag{3}$$

and

$$\{\sigma\}_{pe} = \frac{E_{pe}}{1-\nu_{pe}^2} \begin{bmatrix} 1 & \nu_{pe} & 0 \\ \nu_{pe} & 1 & 0 \\ 0 & 0 & \frac{(1-\nu_{pe})}{2} \end{bmatrix} \begin{Bmatrix} \varepsilon_x^{pl} - \frac{V_{pe}d_{31}}{h_{pe}} \\ \varepsilon_y^{pl} - \frac{V_{pe}d_{32}}{h_{pe}} \\ \varepsilon_{xy}^{pl} \end{Bmatrix}, \tag{4}$$

where E_{pl}, ν_{pl} and E_{pe}, ν_{pe} are the Young's modulus and Poisson ratio of the plate and piezoelectric actuator, respectively.

Note that at all the interfaces between the plate and the piezoelectric elements and at the defective area, the continuity condition of deflection is satisfied. The transverse deflection $w(x, y, t)$ can thereby be approximated by a set of polynomial trial functions as

$$w(x, y, t) = \sum_{i=0}^{m}\sum_{j=0}^{n} A_{ij}(t)\left(\frac{x}{a}\right)^i\left(\frac{y}{b}\right)^j, \tag{5}$$

where $A_{ij}(t)$ are the complex and time-dependent variables to be determined. The given form of equation (5) for the deflection will allow the expression of the kinetic and potential energies in terms of the coefficients A_{ij} and their first-order time derivatives. Using the variational approach, the dynamic response of the plate excited by the piezoelectric actuator can be obtained by solving the Lagrange equations

$$\frac{\mathrm{d}}{\mathrm{d}t}\left(\frac{\partial(T-U)}{\partial \dot{A}_{ij}}\right) - \frac{\partial(T-U)}{\partial A_{ij}} = 0, \tag{6}$$

where T and U are the kinetic energy and potential energy of the system, respectively. Since damage occurring at Ω_d can be regarded as a loss of kinetic energy T, the kinetic energy of the damaged plate with piezoelectric patches is given by

$$T = \frac{1}{2}\int_{V_{pl}} \rho_{pl}\left(1 - \chi_d(x, y)\frac{h_d}{2h}\right)\left(\frac{\partial w}{\partial t}\right)^2 \mathrm{d}V_{pl} + \int_{V_{pe}} \rho_{pe}\left(\frac{\partial w}{\partial t}\right)^2 \mathrm{d}V_{pe}, \tag{7}$$

where ρ_{pl} and ρ_{pe} are the densities of the plate and the piezoelectric patches, respectively; h_d is the depth of the defect and $\chi_d(x, y)$ is the generalized location function of the damage described by the Heaviside function H as

$$\chi_d(x, y) = [H(x - x_{d1}) - H(x - x_{d2})] \times [H(y - y_{d1}) - H(y - y_{d2})]. \tag{8}$$

It is clear that the first term on the right-hand side of equation (7) includes the loss of energy caused by the damage, and the second term contains the effect of piezoelectric patches.

The potential energy U includes energies from the plate, piezoelectric patches, and boundary conditions. Without loss of generality, the potential energy of the plate and the piezoelectric patches can be calculated using

$$U_1 = \frac{1}{2}\int_{V_{pl}} \left(1 - \chi_d(x, y)\frac{h_d}{2h}\right)\{\sigma\}_{pl}^T\{\varepsilon\}_{pl}\,\mathrm{d}V_{pl} + \tfrac{1}{2}\int_{V_{pe}} \{\sigma\}_{pe}^T\{\varepsilon\}_{pe}\,\mathrm{d}V_{pe}. \tag{9}$$

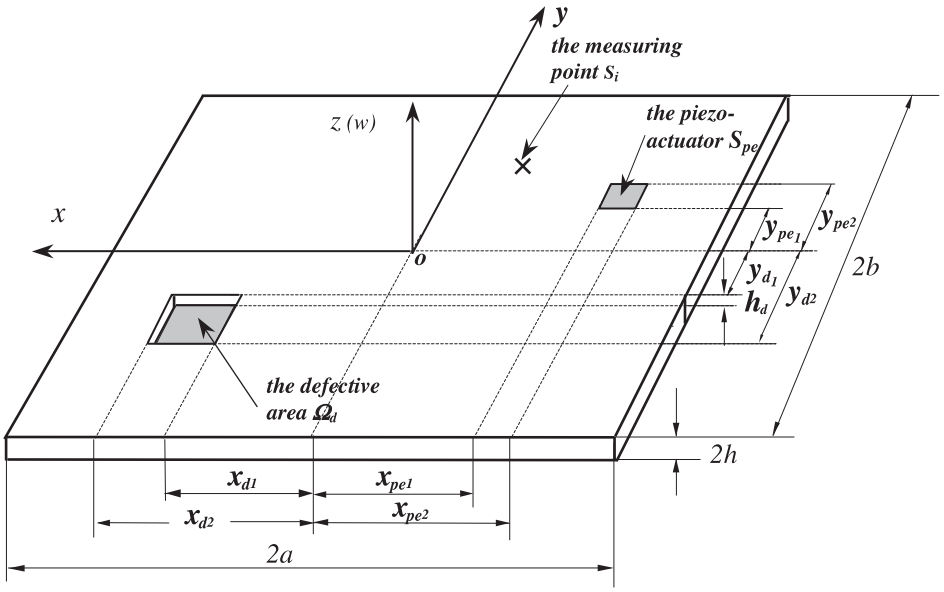

Figure 1. A schematic diagram of a damaged plate with piezoelectric actuation.

Substituting equations (1) to (4) into (9) yields

$$U_1 = \int_{V_{pl}} \frac{E_{pl}z^2}{2(1+v_{pl})}\left\{\frac{1}{(1-v_{pl})}\left(\left(\frac{\partial^2 w}{\partial x^2}\right)^2 + \left(\frac{\partial^2 w}{\partial y^2}\right)^2 + 2v_{pl}\frac{\partial^2 w}{\partial x^2}\frac{\partial^2 w}{\partial y^2}\right) + 2\left(\frac{\partial^2 w}{\partial x\,\partial y}\right)^2\right\} \times \left(1 - \chi_d(x,y)\frac{h_d}{2h}\right) \mathrm{d}V_{pl} + \int_{V_{pe}} \frac{E_{pe}z^2}{2(1+v_{pe})}\left\{\frac{1}{(1-v_{pe})}\left(\left(\frac{\partial^2 w}{\partial x^2}\right)^2 + \left(\frac{\partial^2 w}{\partial y^2}\right)^2 + 2v_{pe}\frac{\partial^2 w}{\partial x^2}\frac{\partial^2 w}{\partial y^2}\right) + 2\left(\frac{\partial^2 w}{\partial x\,\partial y}\right)^2\right\} \mathrm{d}V_{pe} + \int_{V_{pe}} \frac{E_{pe}H_p}{(1-v_{pe}^2)}\,\mathrm{d}V_{pe} \quad (10)$$

where

$$H_p = \left(\frac{V_{pe}}{h_{pe}}\right)^2 [d_{31}^2 + d_{32}^2 + 2v_{pe}d_{31}d_{32}] + \frac{2V_{pe}z}{h_{pe}}\left[\frac{\partial^2 w}{\partial x^2}(d_{31} + v_{pe}d_{32}) + \frac{\partial^2 w}{\partial y^2}(d_{32} + v_{pe}d_{31})\right]. \quad (11)$$

Evidently, the first term on the right-hand side of equation (10) represents the potential energy contributed from the damaged plate; the second term is from the rigidity of the piezoelectric patches, and the last term is the energy supplied by the actuator, which can also be obtained from the integration of the total enthalpy density of the piezoelectric element (Jaffe *et al* 1971).

The boundary conditions of a plate can be simulated by introducing a set of uniformly distributed virtual springs along each edge, and a proper combination of the spring constants can represent all classical boundary conditions (Cheng 1996). Thus, the potential energy related to boundaries is expressed as

$$U_2 = \tfrac{1}{2}\int_{-b}^{b}\Big\{k_1[w(-a,y,t)]^2 + k_2[w(a,y,t)]^2 + c_1\left[\frac{\partial w(-a,y,t)}{\partial x}\right]^2 + c_2\left[\frac{\partial w(a,y,t)}{\partial x}\right]^2\Big\}\mathrm{d}y + \tfrac{1}{2}\int_{-a}^{a}\Big\{k_3[w(x,-b,t)]^2 + k_4[w(x,b,t)]^2 + c_3\left[\frac{\partial w(x,-b,t)}{\partial y}\right]^2 + c_4\left[\frac{\partial w(x,b,t)}{\partial y}\right]^2\Big\}\mathrm{d}x, \quad (12)$$

where $k_1, \ldots, k_4$ are in N m^{-2} for translation and $c_1, \ldots, c_4$ in N rad^{-1} for rotation, all being distributed along the boundaries and therefore having the unit of stiffness over length. Consequently, the total potential energy of the structure is obtained by combining equations (10) and (12) as

$$U = U_1 + U_2. \quad (13)$$

Substituting equations (7) and (13) into Lagrange equation (6) gives the following differential equations:

$$[\boldsymbol{M}]\{\ddot{q}(t)\} + [\boldsymbol{K}]\{q(t)\} = \{B\}V_{pe}, \quad (14)$$

where $\{q(t)\}$ is the generalized coordinate vector to be determined, $[\boldsymbol{M}]$ is the mass matrix derived from the energy terms for the plate ($\boldsymbol{M}^{pl}$), piezoelectric patch ($\boldsymbol{M}^{pe}$), and damage ($\boldsymbol{M}^{da}$), and the elements of matrix $[\boldsymbol{M}]$ are given by

$$M_{pq,rs} = M_{pq,rs}^{pl} + M_{pq,rs}^{pe} - M_{pq,rs}^{da} \quad (0 \leqslant p \leqslant m, 0 \leqslant r \leqslant m, 0 \leqslant q \leqslant n, 0 \leqslant s \leqslant n). \quad (15)$$

The expressions for $M_{pq,rs}^{pl}$ and $M_{pq,rs}^{pe}$ are the same as those given by Proulx (1997) (see appendix). For $M_{pq,rs}^{da}$, one has

$$M_{pq,rs}^{da} = \frac{\rho_{pl}h_d(x_{d2}^{p+r+1} - x_{d1}^{p+r+1})(y_{d2}^{q+s+1} - y_{d1}^{q+s+1})}{a^{p+r}b^{q+s}(p+r+1)(q+s+1)}. \quad (16)$$

$[\boldsymbol{K}]$ is the stiffness matrix obtained by the summation of contributions from the plate ($\boldsymbol{K}^{pl}$), the piezoelectric patch

($\boldsymbol{K}^{pe}$), damage ($\boldsymbol{K}^{da}$), and boundaries ($\boldsymbol{K}^{bords}$). For the $pqrs$th element,

$$K_{pq,rs} = K^{pl}_{pq,rs} + K^{pe}_{pq,rs} + K^{bords}_{pq,rs} - K^{da}_{pq,rs}, \tag{17}$$

where

$$\begin{aligned} K^{da}_{pq,rs} = {} & \frac{E_{pl}(h_d^3 + 3hh_d^2 + 3h^2h_d)}{3(1-\nu_{pl}^2)a^{p+r}b^{q+s}} \\ & \times \left\{ \frac{pr(p-1)(r-1)(x_{d2}^{p+r-3} - x_{d1}^{p+r-3})(y_{d2}^{q+s+1} - y_{d1}^{q+s+1})}{(p+r-3)(q+s+1)} \right. \\ & + \frac{qs(q-1)(s-1)(x_{d2}^{p+r+1} - x_{d1}^{p+r+1})(y_{d2}^{q+s-3} - y_{d1}^{q+s-3})}{(p+r+1)(q+s-3)} \\ & + \{[\nu_{pl}(qr(q-1)(r-1) + ps(p-1)(s-1)) \\ & + 2(1-\nu_{pl})pqrs](x_{d2}^{p+r-1} - x_{d1}^{p+r-1})(y_{d2}^{q+s-1} - y_{d1}^{q+s-1})\} \\ & \left. \times \{(p+r-1)(q+s-1)\}^{-1} \right\} \end{aligned} \tag{18}$$

and the expressions for $K^{pl}_{pq,rs}$, $K^{pe}_{pq,rs}$, and $K^{bords}_{pq,rs}$ are put in the appendix for conciseness. In equation (14), $\{B\}$ is the voltage-to-force transformation vector, whose pqth element b_{pq} is calculated from

$$\begin{aligned} b_{pq} = {} & -\frac{2E_{pe}}{(1-\nu_{pe}^2)a^p b^q} \\ & \times \left[\frac{p}{q+1}(d_{31} + \nu_{pe}d_{32})(x_{pe2}^{p-1} - x_{pe1}^{p-1})(y_{pe2}^{q+1} - y_{pe1}^{q+1}) \right. \\ & \left. + \frac{q}{p+1}(d_{32} + \nu_{pe}d_{31})(x_{pe2}^{p+1} - x_{pe1}^{p+1})(y_{pe2}^{q-1} - y_{pe1}^{q-1}) \right]. \end{aligned} \tag{19}$$

According to equations (15) and (17), it can be found that:

- The effect of damage on the modeling is formulated by a reduction of mass and stiffness through the matrices $\boldsymbol{M}^{da}$ and $\boldsymbol{K}^{da}$. A special case is that when $\boldsymbol{M}^{da}$ and $\boldsymbol{K}^{da}$ become zero; the equations presented will be simplified to the modeling of intact plates.
- The appearance of damage in the region Ω_d in the structure is indicated by the generalized location function $\chi_d(x, y)$, which is embodied in $M^{da}_{pq,rs}$ and $K^{da}_{pq,rs}$. Evidently, different defect areas with the same size and depth, but different defect locations, can lead to different results.
- The effect of damage in matrices $[\boldsymbol{M}]$ and $[\boldsymbol{K}]$ is global. This is different from the finite-element modeling, in which the change of $[\boldsymbol{M}]$ and $[\boldsymbol{K}]$ is local.

In general, the validity of the numerical modeling can be verified by analyzing parameters in the frequency domain or time domain obtained from simulations with those from experiments. It is noted that a parameter, such as the natural frequency, has been extensively utilized to characterize an intact plate with piezoelectric actuators/sensors (Newbury and Leo 2001, St-Amant and Cheng 2000). In the following sections, the feasibility of using natural frequency and time response to characterize a *damaged plate* with piezoelectric actuation is discussed using two related indices for the quantitative analysis.

Table 1. The geometric size and material properties of the specimen.

	Aluminum plate	PZT element
Dimension (m)	0.34×0.24	0.05×0.05
Thickness (m)	2×10^{-3}	5×10^{-4}
Mass density (kg m^{-3})	2700	7650
Young's modulus (Pa)	7.1×10^{10}	6.45×10^{10}
Poisson ratio	0.3	0.3
Piezoelectric constant (e_{31}) (N m V^{-1})	—	1.032×10^{1}
Loss factor	0.01	—

Figure 2. The experimental set-up.

3. Numerical and experimental validations

To illustrate the effectiveness of the modeling approach described above, numerical simulations for a damaged plate with piezoelectric actuation were performed and experimental tests were carried out using the same configuration. The structure used was a damaged aluminum plate containing two surface-bonded piezo-ceramic patches. Dimensions and material properties are tabulated in table 1. The plate was suspended from a stiff steel frame by two nylon bands with very low stiffness to create free boundary conditions. The piezo-ceramics (Sensortech BM500) were bonded on the two opposite sides of the plate at location $\Omega_{pe} : \{-0.055 \leqslant x \leqslant -0.005, 0.007 \leqslant y \leqslant 0.057\}$ using the instant adhesive Loctite 495, and damage was simulated by a defective area $\Omega_d : \{0.1 \leqslant x \leqslant 0.13, -0.06 \leqslant y \leqslant -0.03\}$ with a thickness reduction $h_d = 0.5 \times 10^{-3}$ m. In addition, an intact plate with the same configuration was also processed for comparison.

For the numerical modeling, a software package using *Matlab* was developed, in which the Newmark method was adopted to solve equation (14) (St-Amant and Cheng 2000) to obtain the frequency response function (FRF) and time response. For the experimental testing (figure 2), the exciting signal was generated by a signal generator (TGA 1230), then amplified by a piezo-driver (Trek Model 607), connected to the structure through a pair of piezo-ceramics. The responses of the plate were measured by accelerometers (B&K 4397) and recorded by a signal analyzer (B&K 3023). The data were then analyzed. The electric potential applied on the actuators is 25 V.

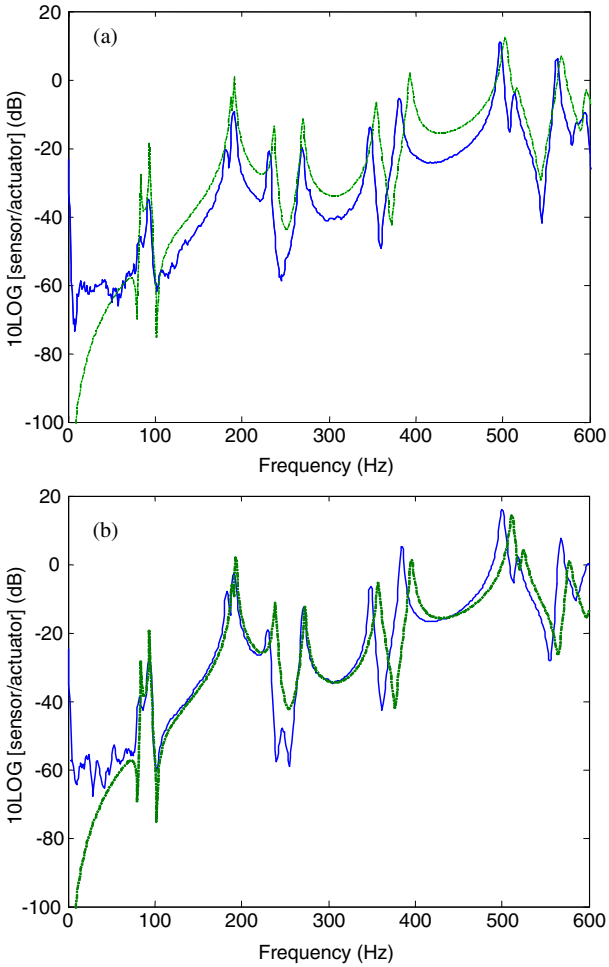

Figure 3. Curves of the FRF. ——: experimental results; · · · · · ·: numerical results. Location of accelerometer: $(-0.106, 0.095)$ (unit: m). (a) Damaged case; (b) intact case.

3.1. Model characterization from the frequency index

When the natural frequency is adopted to characterize a damaged plate, it is generally reflected in the FRF curves. Figure 3(a) shows the FRF curves at the measuring point $(-0.106, 0.095)$, which are obtained from the numerical calculation and experimental test. For experiment, pseudo-random excitation was used to properly cover the whole frequency range of interest. From figure 3(a), it can be observed that:

- Resonant peaks of these two curves are approximately coincident with each other, i.e., natural frequencies obtained from numerical modeling are close to the measured ones.
- The overall trends of the FRF variations are quite similar, although the amplitudes of experimental results are generally slightly lower than those of the numerical ones. This is reasonable, considering the approximate determination of the material damping, and the imperfect bonding between the piezo-ceramic patches and the plate.

As a special case, the modeling of an intact plate is studied by setting $M^{da}_{pq,rs} = 0$ and $K^{da}_{pq,rs} = 0$, and the FRF curves are plotted in figure 3(b). The results have a close resemblance with that obtained for the modeling of the damaged structure. For the sake of clarity, table 2 lists the *first eight* natural frequencies of damaged and intact plates with the piezo-ceramics from numerical modeling, experimental measurement, and finite-element code *Nastran*. The results show that frequencies obtained from the present simulation agree well with those from the test and *Nastran*. In addition, simulations also show a systematic decrease of natural frequencies due to the appearance of damage compared with the intact plate, which is consistent with what is reported in the literature. With the decrease of h_d/h however, the change in frequencies becomes quite small, resulting in a non-obvious variation of the FRF curve. As an example, the FRF curves for the intact ($h_d/h = 0$) and damaged ($h_d/h = 0.05$) cases are plotted in figure 4, which shows a coincidence for the *first two* modes and only a slight shift for the others. In such cases, a quantitative index is required.

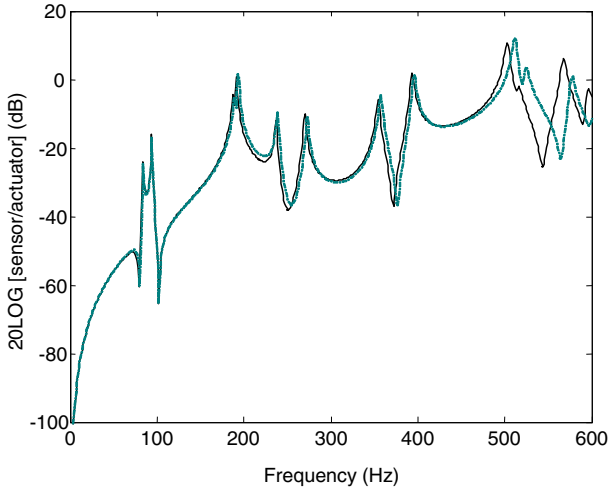

Figure 4. The FRF: solid curve for the damaged case and dashed curve for the intact case.

The relative change of frequency, which is called the frequency index, can be expressed as

$$\Delta f_j = \frac{f_j - \tilde{f}_j}{f_j}, \qquad j = 1, \ldots, m_f, \tag{20}$$

where f_j and $\tilde{f}_j$ are the jth natural frequencies of the intact and damaged structures, respectively; m_f is the number of modes within the analyzed frequency range.

Figure 5 shows Δf for the *first eight* modes (<400 Hz) with h_d/h varying from 0.25 to 0.05. Δf decreases with the reduction of h_d/h; this change is observable even for a small h_d/h. Comparing the curve of Δf for the case of $h_d/h = 0.05$ (marked with 'Δ' in figure 5) with that of the FRF (figure 4) reveals a more quantitative indication when using Δf to characterize the model. Figure 6 compares the simulated and experimental Δf ($h_d/h = 0.25$) for the *first eight* modes, showing similar tendencies in the two cases. It is worth mentioning that the resolution of the FFT analyzer impacts on the accuracy of the test results using Δf.

3.2. Model characterization from the energy index

The occurrence of damage results in a redistribution of structural energy, which can be reflected by the time domain

Table 2. The first eight natural frequencies of the damaged and intact plates with piezo-ceramic actuation.

	Damaged plate			Intact plate		
Mode	Numerical modeling	Experiment	*Nastran*	Numerical modeling	Experiment	*Nastran*
1	83.2	81.5	80.6	83.7	81.9	81.3
2	94.0	92.5	94.5	94.2	93.3	95.4
3	187.8	183.1	184.0	189.6	183.9	188.2
4	191.1	190.4	190.1	193.2	191.5	192.2
5	237.2	232.1	235.0	238.7	233.3	237.4
6	269.8	267.4	272.0	272.6	269.9	278.2
7	354.6	347.3	360.0	357.4	350.0	362.7
8	393.4	382.9	391.5	395.7	385.8	395.1

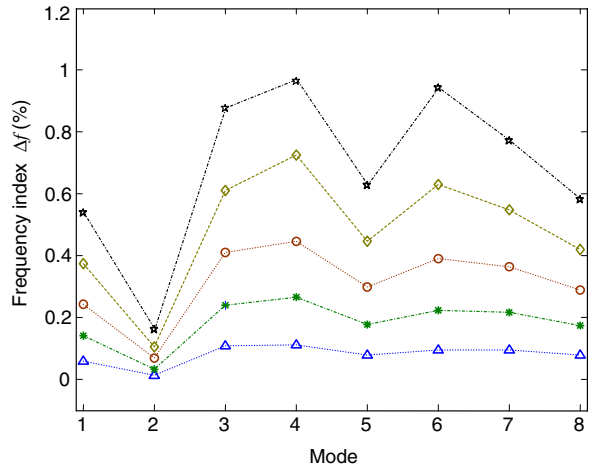

Figure 5. The frequency index Δf with different ratios h_d/h: ★, $h_d/h = 0.25$; ◇, $h_d/h = 0.20$; ○, $h_d/h = 0.15$; ∗, $h_d/h = 0.10$; △, $h_d/h = 0.05$.

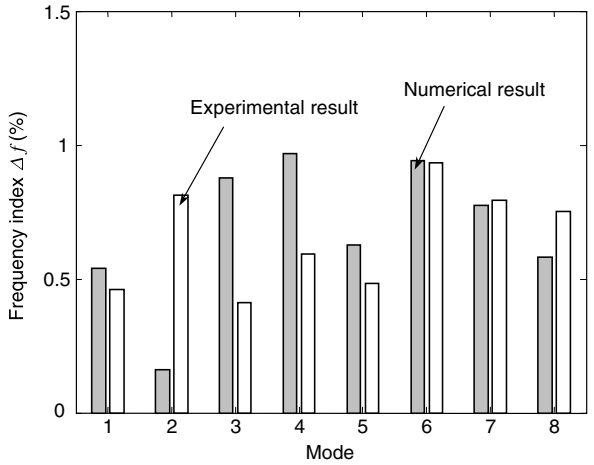

Figure 6. Histograms of the frequency index Δf for the first eight modes: ▭, simulation result; ▭, experimental result.

signal. An energy index is therefore proposed. Considering that the wavelet decomposition can reveal useful information on the signal characteristics that are not apparent in the original signal, it is adopted for signal processing in this study. In general, the signal is decomposed into several wavelet levels. Each level is represented by a set of wavelet coefficients providing localized information. As we know, the integral mean square response (sub-signal) gives the energy distribution among different frequency ranges, which is equivalent to the energy of wavelet transformation at each level. Based on this, an energy index is defined as

$$\Delta E_j = \frac{\tilde{E}_j - E_j}{E_j}, \qquad j = 1, \ldots, m_l, \tag{21}$$

where E_j and $\tilde{E}_j$ are the variances of the orthogonal wavelet coefficients of the jth level for the intact and damaged plate, respectively; m_l is the level depending on the analyzed frequency range and the selection of the order of the wavelet package decomposition. A high level corresponds to a high frequency interval. In this section, the analyzed frequency range is set as (0–800) Hz and the third-order Daubechies wavelets are used. Then, $m_l = 8$ and each level stands for a frequency interval of 100 Hz. For example, *level 8* is related to the frequency range from 701 to 800 Hz.

The feasibility of using an energy index to characterize the model is investigated by analyzing the signals of figures 7(a) and (b), which simulate the responses at point $(-0.106, 0.095)$ by applying a pseudo-random excitation on the intact and damaged ($h_d/h = 0.25$) plates, respectively. No apparent difference can be noticed between the untreated signals (a) and (b). The proposed energy index is then applied. Table 3 lists the energy variation for both intact and damaged cases, in which the change of energy from -16 to 9% for the frequency range considered is found. Figure 8 shows the histogram of simulation results using ΔE_j ($j = 1, \ldots, 8$) with h_d/h varying from 0.25 to 0.05. It can be observed that, for each given range, ΔE_j changes rather regularly with the reduction of h_d/h. Clearly, energy index is more sensitive to damage than both the frequency domain parameters and the untreated time domain signals.

An issue to be addressed is the selection of input signal. Tests and simulations were performed using two types of signal: pseudo-random and square-wave signals. The pseudo-random excitation contains all frequency components and can theoretically excite all modes to give very rich information about system dynamics. The square-wave signals however have a well-defined pattern, ensuring maximum repetitiveness, which can facilitate comparisons.

Figures 9(a) and (b) show the energy index ΔE for the frequency range (0–400) Hz, obtained from numerical simulation and experimental tests using a square-wave signal with the frequency of 80 Hz and a pseudo-random signal, respectively. The measured point was the same as the one used before. These figures show that:

Table 3. The energy index corresponding to figure 7.

Level (Hz)	Energy E_j (intact case)	Energy $\tilde{E}_j$ (damaged case)	ΔE_j (%)
1: 0–100	0.5277	0.5761	9.17
2: 101–200	0.7923	0.7681	−3.05
3: 201–300	0.0880	0.0894	1.59
4: 301–400	0.2826	0.2566	−9.21
5: 401–500	0.0188	0.0203	7.98
6: 510–600	0.0564	0.0590	4.61
7: 601–700	0.0093	0.0078	−16.13
8: 701–800	0.0262	0.0235	−10.31

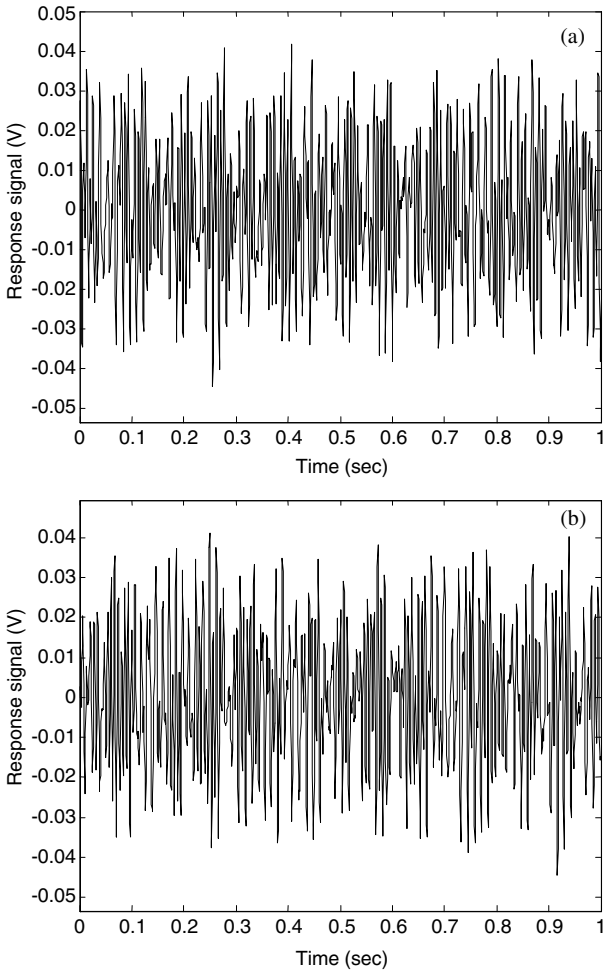

Figure 7. The time response signal at the measurement point (−0.106, 0.095). Input signal: a pseudo-random signal with the frequency range of 0–800 Hz. (a) Intact plate; (b) damaged plate.

- Basically, change in the energy index can be clearly observed. A synchronous change of ΔE for both numerical and experimental approaches appears on using the square-wave signal as input, while a slight tunelessness occurs at level 2 (corresponding to the frequency interval (101–200) Hz) on using the pseudo-random signal. Results show that the square-wave possesses a better repeatability than the pseudo-random signal.
- From figure 9(a), ΔE increases at level 1 and decreases at others, and the tendency of numerical results is consistent with that of the experimental ones. This shows that even with small changes due to the damage, the present model can still simulate the real tendency in energy changes when square-wave excitations are applied. Larger discrepancies occur for levels 1 and 2. One plausible explanation is that, when a square wave is used as excitation, it only contains 80 Hz and its harmonics. In such a case, energy variation

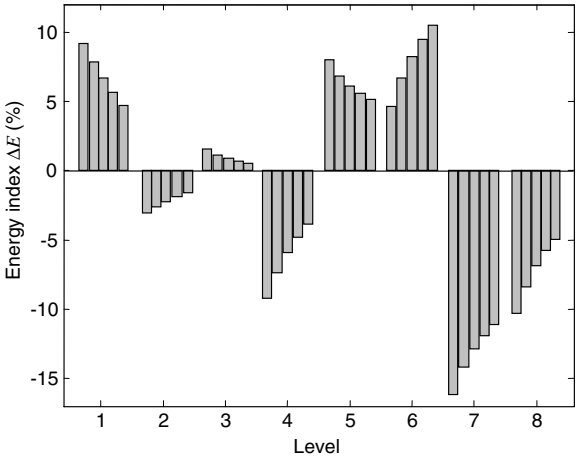

Figure 8. The histogram of the energy index ΔE with h_d/h varying from 0.25 to 0.05.

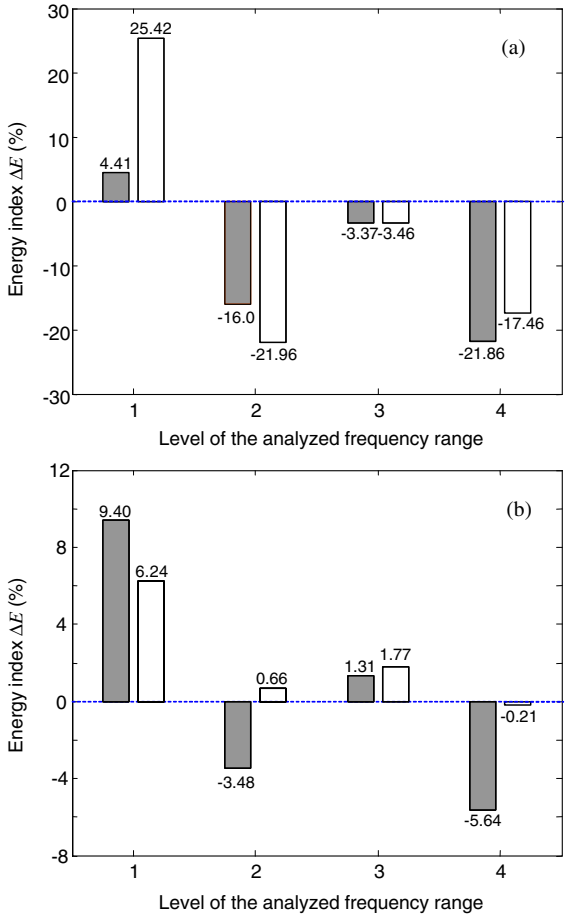

Figure 9. The energy index ΔE obtained at the measurement point (−0.106, 0.095): ▭, simulation result; □, experimental result. (a) Square-wave signal; (b) pseudo-random signal.

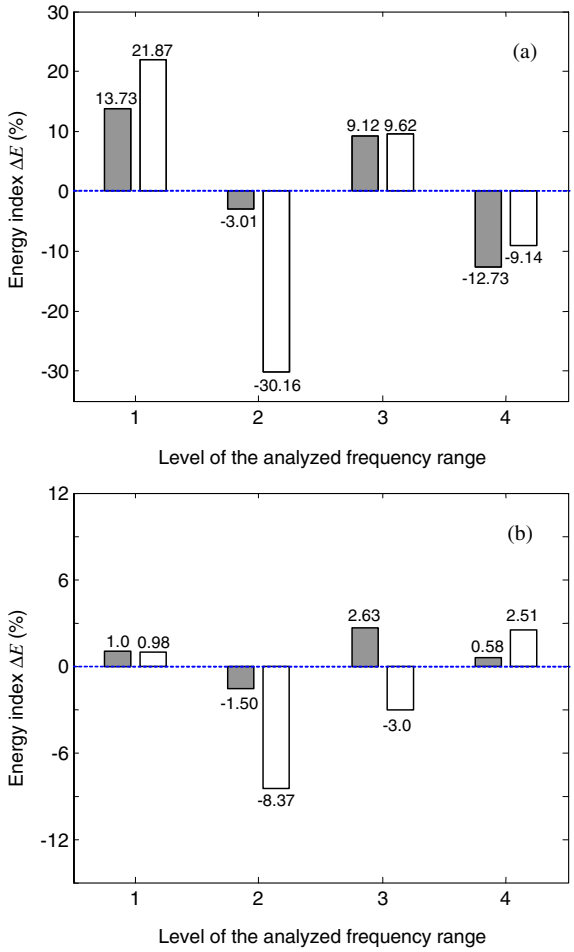

Figure 10. The energy index ΔE obtained at the measurement point $(-0.067, 0.112)$: ▭, simulation result; ▭, experimental result. (a) Square-wave signal; (b) pseudo-random signal.

is only assessed under these frequency components. In experiment, however, low-frequency noise always exists and also leads to energy changes, which cannot be comprehended from simulation. This phenomenon is obviously more apparent for lower frequency ranges:

- The measured maximal ΔE can approach 25%. Comparing the energy index ΔE with the frequency index Δf (figure 5 with a maximal value of about 1%) reveals that the energy index is much more sensitive to damage than the frequency index.

A similar comparison was performed using a different measuring point. Figure 10 illustrates the energy index obtained at point $(-0.067, 0.112)$. All conclusions drawn above also apply to this configuration.

The above analyses show that better results can be obtained using square-wave signals than the pseudo-random signals. The main reason is that the latter cannot be reproduced exactly for different cases; e.g., the excitation signal applied to the intact plate will be different from that applied to the damaged plate. As a result, there is no baseline between the generated response signals. In order to improve this, averaging is applied to the time domain signal to eliminate random error. Figure 11 shows the energy index obtained using

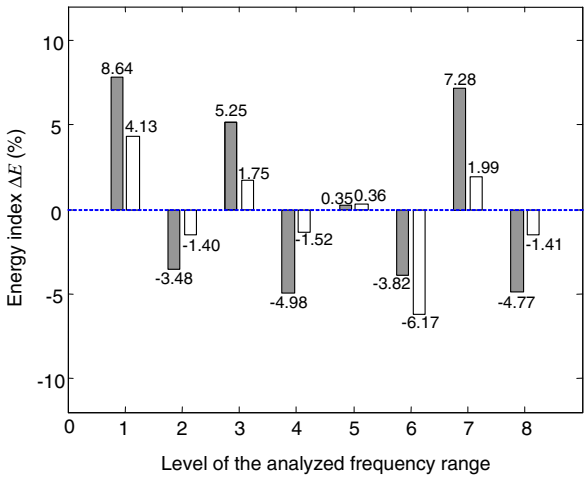

Figure 11. The energy index ΔE obtained at the measurement point $(-0.106, 0.095)$ using the pseudo-random signal with three averagings: ▭, simulation result; ▭, experimental result.

the pseudo-random signal with three averagings performed on the configuration used in figures 9(b). At the same time, the frequency range is also enlarged to cover eight frequency bands up to 800 Hz. It can be seen that the agreements between the test results and the simulation ones are significantly improved and a synchronous change of ΔE appears. Results suggest that, when using the pseudo-random signal as the input, multiple averaging is needed to obtain more reliable results.

4. Conclusions

In this paper, the numerical modeling of a damaged plate with piezoelectric actuation is investigated. The effects of defects are embodied by mass and stiffness reductions in equations of motion. In order to verify the validity of the present modeling, two indices constructed from the frequency variation and energy change are used, and their tendencies obtained from numerical simulation and experimental testing are compared. For the frequency analysis, the pseudo-random signal is generated so as to excite most of the vibration modes of the structure. For the energy analysis, both square-wave and pseudo-random signals can be used to assess the energy index variation with the associated wavelet decomposition technique for signal processing. Numerical simulations and experimental tests show that a good agreement on modeling can be achieved, and the energy index is more sensitive to damage than the frequency index. When pseudo-random excitations are used, an averaging over time signals is needed to provide more reliable results. This study is believed to be of significance because the present model can efficiently simulate dynamic characteristics of a damaged plate with different sizes and locations, which should be useful for establishing databases for future damage detection applications.

Acknowledgment

The authors would like to thank the Research Committee of The Hong Kong Polytechnic University for its financial support for this project (Grant: GYY-27).

Appendix

From the results of Proulx (1997), $M^{pl}_{pq,rs}$ and $M^{pe}_{pq,rs}$ in equation (15) can be expressed as

$$M^{pl}_{pq,rs} = \begin{cases} \dfrac{8\rho_{pl}abh}{(p+r+1)(q+s+1)} \\ \quad \text{for } (p+r) \text{ and } (q+s) \text{ a pair} \\ 0 \qquad \text{otherwise,} \end{cases} \tag{A.1}$$

and

$$M^{pe}_{pq,rs} = \frac{2\rho_{pe}h_{pe}(x^{p+r+1}_{pe2} - x^{p+r+1}_{pe1})(y^{q+s+1}_{pe2} - y^{q+s+1}_{pe1})}{a^{p+r}b^{q+s}(p+r+1)(q+s+1)}. \tag{A.2}$$

Similarly, $K^{pl}_{pq,rs}$, $K^{pe}_{pq,rs}$, and $K^{bords}_{pq,rs}$ in equation (17) take the forms

$$K^{pl} = \begin{cases} \dfrac{8E_{pl}h^3}{3(1-v^2_{pl})}\left[\dfrac{bpr(p-1)(r-1)}{a^3(p+r-3)(q+s+1)}\right. \\ \quad + \dfrac{aqs(q-1)(s-1)}{b^3(q+s-3)(p+r+1)} \\ \quad \left. + \dfrac{v_{pl}[qr(q-1)(r-1)+ps(p-1)(s-1)]+2(1-v_{pl})pqrs}{ab(p+r-1)(q+s-1)}\right] \\ \quad \text{for } (p+r) \text{ and } (q+s) \text{ a pair} \\ \quad 0 \qquad \text{otherwise,} \end{cases} \tag{A.3}$$

$$\begin{aligned} K^{pe}_{pq,rs} = {} & \frac{2E_{pe}(h^3_{pe} + 3hh^2_{pe} + 3h^2h_{pe})}{3(1-v^2_{pe})a^{p+r}b^{q+s}} \\ & \times \left\{ \frac{pr(p-1)(r-1)(x^{p+r-3}_{pe2} - x^{p+r-3}_{pe1})(y^{q+s+1}_{pe2} - y^{q+s+1}_{pe1})}{(p+r-3)(q+s+1)} \right. \\ & + \frac{qs(q-1)(s-1)(x^{p+r+1}_{pe2} - x^{p+r+1}_{pe1})(y^{q+s-3}_{pe2} - y^{q+s-3}_{pe1})}{(p+r+1)(q+s-3)} \\ & + \{(v_{pe}(qr(q-1)(r-1)+ps(p-1)(s-1))+2(1-v_{pe})pqrs) \\ & \left. \times (x^{p+r-1}_{pe2} - x^{p+r-1}_{pe1})(y^{q+s-1}_{pe2} - y^{q+s-1}_{pe1})\}\{(p+r-1)(q+s-1)\}^{-1} \right\} \end{aligned} \tag{A.4}$$

and

$$\begin{aligned} K^{bords}_{pq,rs} = 2\Bigg\{ & \frac{b[(-1)^{p+r}k_1 + k_2 + \frac{pr}{a^2}((-1)^{p+r-2}c_1 + c_2)]}{q+s+1} \\ & + \frac{a[(-1)^{q+s}k_3 + k_4 + \frac{qs}{b^2}((-1)^{q+s-2}c_3 + c_4)]}{p+r+1} \Bigg\}. \end{aligned} \tag{A.5}$$

References

Agrawal S K, Tong D Q and Nagaraja K 1994 Modeling and shape control of piezoelectric actuator embedded elastic plates *J. Intell. Mater. Syst. Struct.* **5** 514–21

Banks H T, Emeric P and Plancke C 1997 Modeling of nonsymmetrical damage in plate-like structures *Math. Comput. Modelling* **26** 55–65

Banks H T, Smith R C and Wang Y 1995 The modeling of piezoceramic patch interactions with shells, plates, and beams *Q. Appl. Math.* **53** 353–81

Barbero E J and Reddy J N 1991 Modeling of delamination in composite laminates using a layer-wise plate-theory *Int. J. Solids Struct.* **28** 373–88

Benjeddou A 2000 Advances in piezoelectric finite element modeling of adaptive structural elements: a survey *Comput. Struct.* **76** 347–63

Bhattacharya P, Suhail H and Sinha P K 1998 Finite element free vibration analysis of smart laminated composite beams and plates *J. Intell. Mater. Syst. Struct.* **9** 20–8

Chandrashekhara K and Smyser C P 1998 Dynamic modeling and neural control of composite shells using piezoelectric devices *J. Intell. Mater. Syst. Struct.* **9** 29–43

Chattopadhyay A, Gu H Z and Dragomir-Daescu D 1999 Dynamics of delaminated composite plates with piezoelectric actuators *AIAA J.* **37** 248–54

Chee C Y K, Tong L Y and Steven G P 1998 A review on the modeling of piezoelectric sensors and actuators incorporated in intelligent structures *J. Intell. Mater. Syst. Struct.* **9** 3–19

Chee C Y K, Tong L Y and Steven G P 1999 A mixed model for composite beams with piezoelectric actuators and sensors *Smart Mater. Struct.* **8** 417–32

Cheng L 1996 Vibroacoustic modeling of mechanically coupled structures: artificial spring technique applied to light and heavy mediums *Shock Vib.* **3** 193–200

Fuller C R, Elliott S J and Nelson P A 1996 *Active Control of Vibration* (London: Academic)

Gopinathan S V, Varadan V V and Varadan V K 2000 A review and critique of theories for piezoelectric laminates *Smart Mater. Struct.* **9** 24–48

Heyliger P and Saravanos D A 1995 Exact free-vibration analysis of laminated plates with embedded piezoelectric layers *J. Acoust. Soc. Am.* **98** 1547–57

Jaffe B, Cook W and Jaffe H 1971 *Piezoelectric Ceramics* (London: Academic)

Jian X H, Tzou H S, Lissenden C J and Penn L S 1997 Damage detection by piezoelectric patches in a free vibration method *J. Compos. Mater.* **31** 345–59

Lam K Y and Ng T Y 1999 Active control of composite plates with integrated piezoelectric sensors and actuators under various dynamic loading conditions *Smart Mater. Struct.* **8** 223–37

Newbury K M and Leo D J 2001 Structural dynamics of stiffened plates with piezoceramic sensors and actuators *AIAA J.* **39** 942–50

Ostachowicz W and Krawczuk M 2001 On modeling of structural stiffness loss due to damage *Damage Assessment Struct.: Key Eng. Mater.* **204** 185–99

Proulx B 1997 Développement d'un modèle de simulation sur le contrôle actif d'une plaque mince avec des céramiques piézoélectriques *Master Thesis* Laval University, Québec, Canada

Proulx B and Cheng L 2000 Dynamic analysis of piezoceramic actuation effects on plate vibrations *Thin-Walled Struct.* **37** 147–62

Qu Z Q 2001 An efficient modelling method for laminated composite plates with piezoelectric sensors and actuators *Smart Mater. Struct.* **10** 807–18

St-Amant Y and Cheng L 2000 Simulations and experiments on active vibration control of a plate with integrated piezoceramics *Thin-Walled Struct.* **38** 105–23

Wang S Y, Quek S T and Ang K K 2001 Vibration control of smart piezoelectric composite plates *Smart Mater. Struct.* **10** 637–44